Supplementary Material (ESI) for Soft Matter

Supporting Information

Spontaneous Symmetry Breaking: Formation of Janus Micelles

Ilja K. Voets,[†] Remco Fokkink,[†] Thomas Hellweg,[§] Stephen M. King,[¤] Pieter de Waard,[¥] Arie de Keizer,[†] and Martien A. Cohen Stuart[†]*

[†]Laboratory of Physical Chemistry and Colloid Science, Wageningen University, Dreijenplein 6, 6703 HB Wageningen, The Netherlands

[§]Physikalische Chemie I, University of Bayreuth, 95440 Bayreuth, Germany

[¤]ISIS facility, Rutherford Appleton Laboratory, Chilton, Didcot, Oxon, England

[¥]Wageningen NMR Centre, Wageningen University, Dreijenlaan 3, 6703 HA Wageningen, The Netherlands

*ilja.voets@wur.nl; remco.fokkink@wur.nl; thomas.hellweg@tu-berlin.de; smk@isise.rl.ac.uk; pieter.dewaard@wur.nl; arie.dekeizer@wur.nl; martien.cohenstuart@wur.nl

1 Experimental section

1.1 Materials

The synthesis of the block copolymers poly(*N*-methyl-2-vinyl pyridinium iodide)-*block*-poly(ethylene oxide), $P2MVP_{42}$-*b*-PEO_{446} and poly(acrylic acid)-*block*-poly(acryl amide), PAA_{42}-*b*-$PAAm_{417}$ has been described elsewhere.[1, 2] Briefly, $P2VP_{42}$-*b*-PEO_{446} has been synthesised by sequential anionic polymerisation[3] (polydispersity index, PDI ~ 1.02), followed by quaternisation with methyl iodide (degree of quaternisation ~ 89%), while PAA_{42}-*b*-$PAAm_{417}$ has been synthesised by RAFT according to the MADIX process (PDI ~ 1.3). Chemical structures are given in Scheme S1, subscripts correspond to the degree of polymerisation.

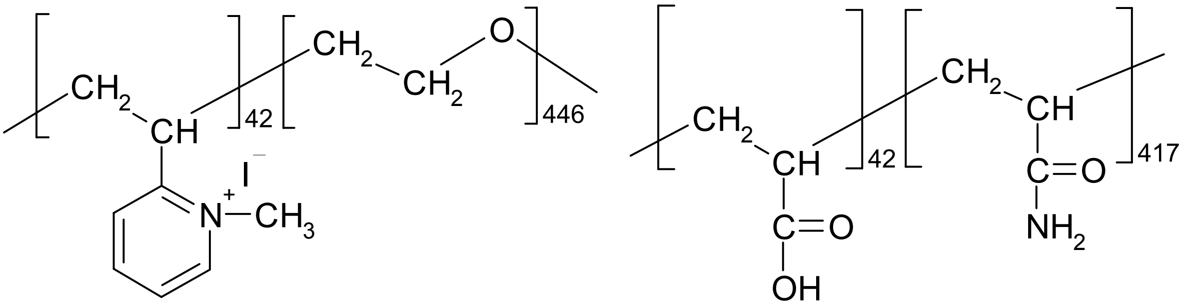

Scheme S1. *Chemical structure of the diblock copolymers $P2MVP_{42}$-b-PEO_{446} (left) and PAA_{42}-b-$PAAm_{417}$ (right). The numbers beside the brackets denote the degree of polymerisation.*

Aqueous polymer stock solutions were prepared by addition of $NaNO_3$ to Milli-Q water or D_2O (> 99% isotope purity, Aldrich), followed by dissolution of the polymer, and subsequent p*H*-adjustment using 0.1 and 1.0 M NaOH and HNO_3. C3Ms were prepared by mixing the $P2MVP_{42}$-*b*-PEO_{446} and PAA_{42}-*b*-$PAAm_{417}$ stock solutions at the preferred micellar composition, PMC, corresponding to a 1:1 ratio of chargeable groups; *i.e.*, a mixing fraction of 0.5, for $pH = 7.7$. The mixing fraction, f_+ is defined as the ratio between the number of positively chargeable monomers and the sum of the numbers of positively and negatively chargeable monomers, *i.e.*,

$$f_+ = \frac{[n_+]}{[n_+]+[n_-]} \qquad (0.1)$$

Unless otherwise specified, all experiments were performed in H_2O (D_2O for SANS, ^1H NMR, and some light scattering experiments) at p*H* (p*D*) = 7.7, 1 mM $NaNO_3$, $f_+ = 0.5$, and 25.0 ºC. In D_2O, we corrected the measured pH_{app} value according to the known shift in proton activity upon 100% substitution of hydrogen into deuterium, *i.e.*, 0.408, to obtain the p*D*.[4] For light scattering experiments, polymer stock solutions were filtered over a 0.20 / 0.45 μm Acrodisc / Schleicher and Schuell filter prior to mixing. All polymers and other chemicals were used as received, without further purification.

1.2 Light scattering-titrations (LS-T)

The experimental setup and data analysis procedures have been detailed in a previous publication.[5] Results are given as total light scattering intensity, I_{90°, divided by the polymer concentration, C_p, and hydrodynamic radius, $R_{h,\,90^\circ}$ at a scattering angle of 90º as a function of f_+. During the mole fraction titrations, a PAA_{42}-*b*-$PAAm_{417}$ solution in the scattering cell (~ 1 g l^{-1}), was titrated with a concentrated solution of $P2MVP_{42}$-*b*-PEO_{446} (~ 9 g l^{-1}), to minimise dilution effects. During the salt titrations, a ~ 3.6 M $NaNO_3$ solution, and during the p*H* titrations, a 0.01 or 0.1 M NaOH or HNO_3 solution, was added to a 1:1 mixture of PAA_{42}-*b*-$PAAm_{417}$ and $P2MVP_{42}$-*b*-PEO_{446}.

1.3 Static and dynamic light scattering (SLS / DLS)

Static and dynamic light scattering measurements have been performed on an ALV light scattering instrument with an ALV-5000 digital correlator and a Spectra Physics 2000 1 W argon ion laser operated at a wavelength of 514.5 nm. A refractive index matching bath of filtered *cis*-decalin surrounded the cylindrical scattering cell, and the temperature was controlled at 25.0 ± 0.3 ºC using a Haake F8-C35 thermostat. The second-order correlation function, $G_2(t)$ and total averaged scattered intensity were recorded 5 times per angle, for 24 angles, θ, from 30˚ to 145˚ in increments of 5˚ to evaluate the angular dependence of the diffusion coefficient, D, and the excess Rayleigh ratio, $R(\theta,C)$. DLS experiments have been analysed using the method of cumulants and inverse Laplace transformation (CONTIN software). The diffusion coefficient extrapolated to zero angle, D^0, has been obtained from the slope in a plot of the average frequency, Γ versus q^2 and has been calculated into a hydrodynamic radius, R_h^0 via the Stokes-Einstein equation.

The excess Rayleigh ratio, $R(\theta,C)$ can be calculated from the measured sample scattering, I_{sample}, solvent scattering, $I_{solvent}$, toluene scattering (toluene was used as a reference), I_{toluene}, and the excess Rayleigh ratio of toluene, $R(\theta)_{\text{toluene}}$, being 3.2 10^{-5} cm^{-1}, according to

$$R(\theta,C)=\frac{I_{sample}-I_{solvent}}{I_{toluene}}R(\theta)_{toluene} \qquad (0.2)$$

On the other hand, the experimentally accessible quantity $R(\theta,C)$ is linked to the molecular characteristics of the scattering particles according to the general equation

$$R(\theta,C)=KC_{part}M_{part}P(q)S(q) \qquad (0.3)$$

with the weight concentration of scattering particles, C_{part}, the molar mass of the scattering particles, M_{part}, the form factor, $P(q)$, the structure factor, $S(q)$, and an optical constant, K, being

$$K=\frac{4\pi^2n^2}{N_{\text{av}}\lambda_0^4}\left(\frac{dn}{dc}\right)^2 \qquad (0.4)$$

with the solvent refractive index, n, the laser wavelength (514.5 nm), λ_0, Avogadro's number, N_{av}, and the specific refractive index increment, dn/dc, estimated at ~ 0.181 cm^3 g^{-1} for the C3Ms in this study, and the magnitude of the scattering wave vector, q, being

$$q=\frac{4\pi n}{\lambda_0}\sin\left(\frac{\theta}{2}\right) \qquad (0.5)$$

SLS experiments have been analysed in terms of the Zimm and Guinier approximation to equation (0.3), to yield the apparent micellar mass, M_{micel}, radius of gyration extrapolated to zero angle, R_g^0, and apparent micellar aggregation number, P_{agg}.

1.4 Small angle neutron scattering (SANS)

SANS measurements were performed on the LOQ diffractometer at the ISIS pulsed neutron source at the Rutherford Appleton Laboratory in the scattering vector range of 0.008 to 0.25 Å^{-1}. The samples were contained in Hellma 5 mm path length quartz cells and maintained at a temperature of 25 °C. The data were corrected for background scattering, detector response, the spectral distribution of the incident neutron beam, and converted to an absolute scattering cross-section $I(q)$ / cm^{-1} using standard ISIS procedures. Data analysis was performed with software packages such as macros for IGOR PRO provided by NIST[6] and GIFT[7].

The q-dependence of the absolute scattering cross-section can be written as[8, 9]

$$I(q) = n_{part}(\rho_{part} - \rho_{solv})^2 V_{part}^2 P(q) S(q)\text{, and} \tag{0.6}$$

$$I(q) = 4\pi\int_0^\infty p(r)\frac{\sin(qr)}{qr}dr, \tag{0.7}$$

with the particle number density, n_{part} / cm^{-3}, the particle coherent scattering length density, ρ_{part} / cm^{-2}, the solvent coherent scattering length density, ρ_{solv} / cm^{-2}, the particle volume, V_{part} / cm^3, the pair distance distribution function, p(r) / cm^{-2} and the magnitude of the scattering vector, q, as defined in equation (0.5), with the wavelength of the incident radiation, λ_0, the angle between the scattered and incident beam, θ, and $n = 1$.

The pair distance distribution function can be obtained easily by indirect Fourier transformation of equation (0.7). The radius of gyration can be obtained from the GIFT results by applying[9]

$$R_g^2 = \frac{1}{2}\frac{\int_0^{D_{\max}} p(r)r^2 dr}{\int_0^{D_{\max}} p(r)dr} \tag{0.8}$$

Alternatively, a suitable form and structure factor may be selected to be substituted into equation (0.6). Here, we assume $S(q)$ to be unity, as dilute solutions are measured, while several form factors (including $P(q)$ for homogeneous spheres, core-shell spheres, oblate ellipsoids, prolate ellipsoids) were attempted to fit the data. The particle mass, M_{part} / g mol^{-1} can be obtained from the forward scattering intensity at $q = 0$, I_0 / cm^{-1}, according to

$$I_0 = \frac{M_{part} C_{part} (\rho_{bb} - \rho_{solv})^2 v_0^2}{N_{av}}, \tag{0.9}$$

with the particle weight concentration, C_{part} / g cm^{-3}, the building block coherent scattering length density, ρ_{bb} / cm^{-2}, and the building block specific volume, v_0 / cm^3 g^{-1}. The number of PAA$_{42}$-*b*-PAAm$_{417}$ polymers, P_{agg}^-, and P2MVP$_{42}$-*b*-PEO$_{446}$ polymers, P_{agg}^+ per particle, can now easily be obtained by division of the particle molar mass, M_{part}, by the building block molar mass, M_{bb}. For the C3Ms in this study, we define a building block as a neutral unit consisting of one PAA$_{42}$-*b*-PAAm$_{417}$ polymer and one P2MVP$_{42}$-*b*-PEO$_{446}$ polymer, *i.e.*, $f_+ = 0.5$. A building block is present $P_{\text{agg}} = P_{\text{agg}}^+ = P_{\text{agg}}^-$ times in one particle. An overview of the coherent scattering length densities, ρ, specific volume, v_0, dn/dc, and molecular weights, M_w of the monomers, solvent, and C3M building blocks are given in Table S1.

Table S1. *Molecular weight,* M_w */ g mol*$^{-1}$*, specific volume,* v_0 */ cm*^{3} *g*$^{-1}$*, specific refractive index increment,* dn/dc */ cm*^{3} *g*$^{-1}$*, and coherent neutron,* ρ_N*, and X-ray,* ρ_X*, scattering length density / 10*^{10} *cm*$^{-2}$*.*

Species	M_w	v_0	dn/dc	ρ_N	ρ_X
D_2O	20.00	0.905	nd	6.37	9.34
PAAm in H_2O	71.08	0.741	0.187[10]	1.88	12.21
PAAm in D_2O	73.06	0.741	nd	4.15	11.88
PEO	44.05	0.834[10]	0.136 ± 0.003[10]	0.68	11.05
PAA$^-$	71.05	0.951	0.261[11]	1.81	9.26
P2MVP$^+$	120.17	0.952	0.27[11]	1.33	9.61
P2VP$^+$ in H_2O	106.15	0.952	0.27[11]	1.55	9.55
P2VP$^+$ in D_2O	107.14	0.952	nd	2.15	9.46
C3Ms in H_2O	57254	0.798	1.181	1.40	11.40
C3Ms in D_2O	58086	0.798	nd	2.51	11.24

Values are given for polyelectrolyte species in charged state. $P2MVP_{42}$*-b-*PEO_{446} *is assumed to be 89% quaternised. The specific volume and specific refractive index increment of P2MVP*$^+$ *have been approximated by those of P2VP. As* D_2O *samples have been prepared several days prior to measurement and the amount of deuterons far exceeds the amount of protons, it is assumed that all* NH_2 *groups in* D_2O *have been converted into* ND_2 *groups due to exchange of label amide protons with solvent deuterons.*

1.5 Small angle X-ray scattering (SAXS)

SAXS experiments were performed on a SAXSess camera (Anton-Paar, Graz, Austria) using an X-ray generator (Philips, PW 1730/10) operated at 40 kV and 50mA with a sealed-tube Cu anode. A Göbel mirror was used to convert the divergent polychromatic X-ray beam into a collimated line-shaped beam of Cu Kα radiation (λ = 0.154 nm). The 2D scattering pattern, as recorded on a two-dimensional imaging phosphor storage plate, was integrated to yield $I(q)$ versus q using SAXSQuant software (Anton-Paar). The sample holder consisted of a quartz capillary in a metal block, temperature controlled by a

Peltier element at ± 0.1 °C. Electron densities are given in Table S1.

1.6 Cryogenic transmission electron microscopy (cryo-TEM)

Cryo-TEM observations were carried out at 100K on a Philips CM12 Microscope operating on at 120kV. Samples were prepared on Quantifoil® grids (R2/2, 200 mesh grids with a pattern of 2 μm holes in a support film) using the Vitrobot®. Images were taken under low dose conditions.

1.7 2D ^{1}H NMR nuclear Overhauser effect spectroscopy (2D ^{1}H NOESY NMR)

Nuclear Overhauser effect spectroscopy is a two-dimensional NMR technique probing internuclear distances by means of the nuclear Overhauser effect (NOE). A more detailed introduction to the technique has been given in a previous paper.[12] ^{1}H NMR spectra of the C3M solutions were recorded at 298K on a Bruker AMX-500 spectrometer, operating at 500 MHz, located at the Wageningen NMR Centre. For the 2D NOESY spectrum 976 experiments of 2048 data points were recorded, using standard Bruker software. The mixing time was 500 ms.

2 Results and Discussion

2.1 Preparation of Janus Micelles

DLS and SLS experiments have been performed to characterize the Janus micelles in terms of their size, mass, and aggregation number. Results are given in Figure 1 in the main text, Figure S1, and Table S2. The presence of a (small) number of large (loose) aggregates hampers quantitative data analysis and introduces an additional systematic uncertainty in the tabulated values. A limited θ-range of 75 - 120° has been considered for the SLS experiments, as upturns were observed for smaller angles, assuming that the high q scattering is predominately stemming from the Janus micelles, and not aggregates thereof. The fast mode observed in the DLS experiments, shows a q^2-dependent behaviour, while the behaviour of Γ / q^2 is not clearly q-independent, which may be caused by for example, polydispersity or non-spherical morphology. We obtain rather high values of R_g/R_h (R_g/R_h = 0.775 for uniform hard spheres), in the range of 0.9 - 1.2, which have been reported for star-like spherical micelles[13, 14] and non-spherical, elongated objects,[14] such as ellipsoids. Hence, these results may again be caused by the non-spherical shape of the particles, but it is rather tricky to deduce micellar morphology from these data, especially since the R_h and R_g values are corrected differently for the presence of aggregates.

Extrapolation of $R(\theta,C)$ to zero concentration results in estimates for the second virial coefficient, A_2, of $8.3 \cdot 10^{-5}$ m^3 mol kg^{-2} (Guinier and Zimm extrapolation) and $9.8 \cdot 10^{-5}$ m^3 mol kg^{-2} (Debye analysis, *i.e.*, extrapolation to zero concentration, at θ = 90°). However, these values are to be taken as very rough estimates, due to the limited concentration range studied (0.32 - 1.71 g l^{-1}).

Table S2. *Light scattering results for 1:1 aqueous mixtures of* PAA_{42}-*b*-$PAAm_{417}$ *and* $P2MVP_{42}$-*b*-PEO_{446}. *Experimental error is estimated at about 10 - 15%. Radii / nm,* M_w */ kg mol*$^{-1}$, C_p */ g l*$^{-1}$, *and* D^0 */* 10^8 *cm*^{2} *s*$^{-1}$.

Solvent	f_+	C_p	D^0	R_h^{0a}	M_w^b	M_w^c	P_{agg}^b	P_{agg}^c	R_g^{0b}	R_g^{0c}	$R_g^0/R_h^{0\,b}$	$R_g^0/R_h^{0\,c}$
D_2O	0.52		10.6	18.5								
H_2O	0.50	1.71	14.5	17.1	457	459	7.9	7.9	19.1	19.8	1.1	1.2
H_2O	0.50	1.45			471	472	8.1	8.1	18.8	19.5	1.1	1.1
H_2O	0.50	0.32			541	541	9.3	9.3	15.6	15.9	0.9	0.9

[a]*CONTIN analysis,* [b]*Guinier analysis,* [c]*Zimm analysis*

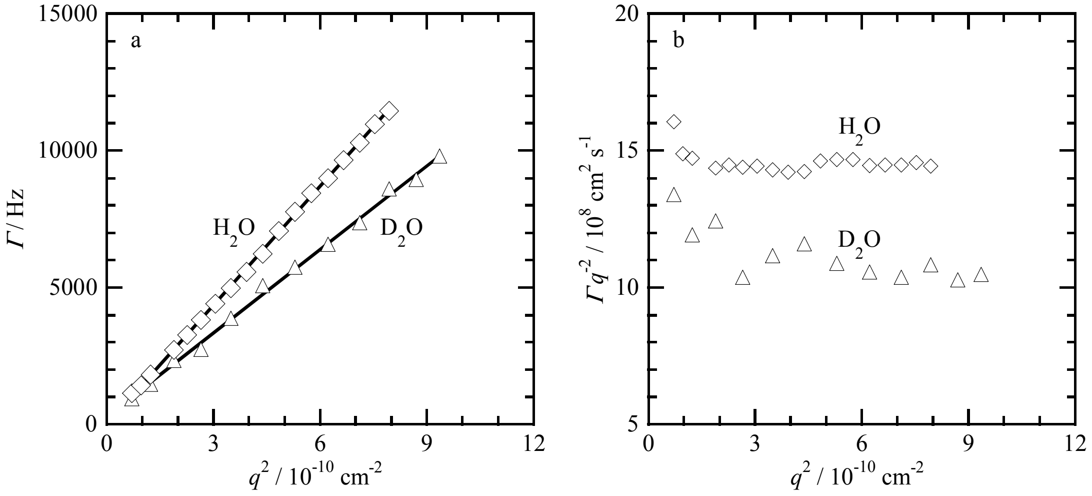

Figure S1. *Results of a CONTIN analysis. (a)* Γ */ Hz as a function of* q^2 *(fast mode), and (b)* Γ/q^2 */* 10^8 *cm*^{2} *s*$^{-1}$ *as a function of* q^2 *for a 1:1 mixture of* PAA_{42}-*b*-$PAAm_{417}$ *and* $P2MVP_{42}$-*b*-PEO_{446} *(◊:* f_+ = *0.5, C = 1.71 g l*$^{-1}$, H_2O; *Δ:* f_+ = *0.52, C = 1.01 g l*$^{-1}$, D_2O*). Lines indicate linear fits to the experimental data.*

Just like from SLS experiments, the radius of gyration, the micellar mass, and the aggregation number can be obtained from SANS and SAXS scattering curves when the data are brought to absolute scale. Table S3 presents an overview of the molecular characteristics obtained from the different methods of data analysis (see manuscript for details). The SANS values for M_{part} and P_{agg} are comparable to the SLS values, but the SAXS values are considerably lower. A tentative explanation may be the presence of a non-negligible amount of counterions in the micellar core, leading to incorrect coherent X-ray scattering length densities. The small values of R_g and R_g/R_h^0 result from the low shell contrast, as discussed previously for C3Ms of PAA_{42}-*b*-PAAm_{417} and $\mathrm{P2MVP}_{209}$.[15]

Table S3. *SANS and SAXS results for C3Ms of* PAA_{42}-*b*-PAAm_{417} *and* $\mathrm{P2MVP}_{42}$-*b*-PEO_{446} *in* D_2O *(pD = 7.8,* $C_p = 4.19$ *g* l^{-1}*). Experimental data and fits are given in Figures 3 and S2. We estimate the uncertainties in* M_{part} */ kg* mol^{-1} *and* P_{agg} *to be in the order of 10 - 15%, considering standard uncertainties in their calculation, such as those in the determination of the scattering length densities. The incoherent scattering (of solvent and hydrogenated polymer segments) of* $7 \cdot 10^{-3}$ cm^{-1} *was subtracted from the SANS scattering curves. Radii are given in nm,* I_0 / cm^{-1}.

Experiment	Analysis	$R_g, \langle R \rangle$	I_0	M_{part}	P_{agg}	R_g/R_h^0
SANS	Guinier	11.9	1.98	324	6	0.64
	Model	-	2.12	348	6	-
	GIFT	12.1	-	-	-	0.66
SAXS	Guinier	9.04	0.24	163	3	0.49
	Model	-	0.24	163	3	-
	GIFT	11.9	-	-	-	0.64

The hydrodynamic radii of C3Ms obtained through a mole fraction titration, p*H* titration, and direct mixing are compared to evaluate whether the micelles are equilibrium structures. If they are, $R_{h,\,90^\circ}$ should be independent of the preparation method. Table S4 shows that for a given solvent, $R_{h,\,90^\circ}$ obtained for C3Ms prepared according to different protocols are indeed identical within experimental error. Furthermore, as a CONTIN analysis (where the aggregates are considered separately) results in a marginal difference in $R_{h,\,90^\circ}$ for C3Ms in D_2O compared to C3Ms in H_2O, we conclude that the effect of solvent deuteration on C3M size is negligible. The cumulant values for C3Ms in D_2O are slightly higher, due to the presence of aggregates.

Table S4. *Hydrodynamic radii, $R_{h,\ 90°}$ / nm for 1:1 mixtures of PAA_{42}-b-$PAAm_{417}$ and $P2MVP_{42}$-b-PEO_{446} in H_2O and D_2O obtained through a mole fraction LS-T, a pH LS-T, and direct mixing.*

Preparation Method	Solvent	$R_{h,\ 90°}$ [a]	$R_{h,\ 90°}$ [b]
direct mixing	D_2O	19.6	18.1
p*H* LS-T	D_2O	20.8 ± 2.2[c]	18.5 ± 0.5[c]
direct mixing	H_2O	17.3	16.9
f_+ LS-T	H_2O	17.6	17.8

[a]*Cumulant analysis,* [b]*CONTIN analysis,* [c]*averaged value for pH > 5.7*

2.2 Characterization of Janus Micelles

Figure S2 clearly shows that a model for polydisperse oblate ellipsoids can be used to accurately describe the neutron and X-ray scattering data.

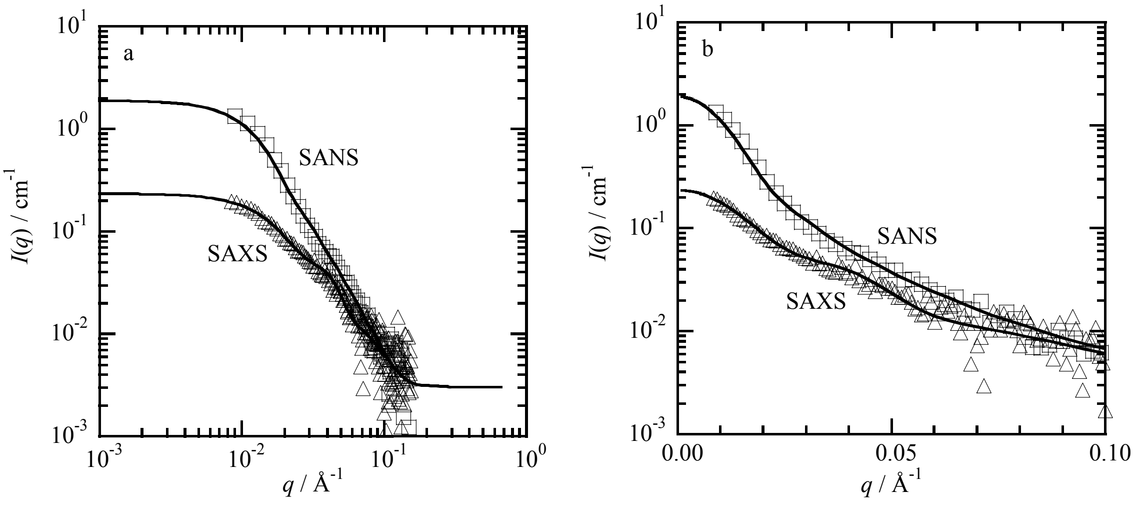

Figure S2. *Model fitting of the SANS (□) and SAXS (Δ) experiments shown in Figure 3 of the main text. $I(q)$ / cm^{-1} versus q / Å^{-1} on double log scale (a) and log lin scale (b). Scattering curves were corrected for solvent scattering. Markers correspond to experimental data; solid lines represent fits with a model for monodisperse oblate ellipsoids.*

To study the proximity of PEO and PAAm chains within the micellar corona directly, two-dimensional proton NMR nuclear Overhauser effect spectroscopy experiments (2D ^{1}H NMR NOESY) were performed (Figure S3). Off-diagonal cross-peaks should appear for nearby unlike protons, *i.e.*, within 0.5 nm, as observed previously for C3Ms of PAA_{42}-*b*-$PAAm_{417}$ and $PDMAEMA_{45}$-*b*-$PGMA_{90}$.[12] The circles in Figure S3 mark the positions where such cross-peaks between the coronal blocks PAAm and PEO should occur. Clearly, no significant peaks are observed. More quantitatively, the area under the intramolecular PAA-*b*-PAAm cross-peaks is about 5 - 30% of the corresponding diagonal peak, while nothing > 0.2% is observed at the encircled positions (Figure S4); i.e., the potential PAAm / PEO cross-peak (1.64 / 3.65 ppm) is not significantly above the noise level, while the intramolecular cross-peaks between PAAm / PAA (1.64 / 2.29 ppm) and PAAm / PAAm (1.64 / 2.16 ppm) clearly are. As PEO and PAAm are both highly flexible,* we may conclude that the blocks indeed avoid each others presence, *i.e.*, PEO and PAAm chains tend to segregate.

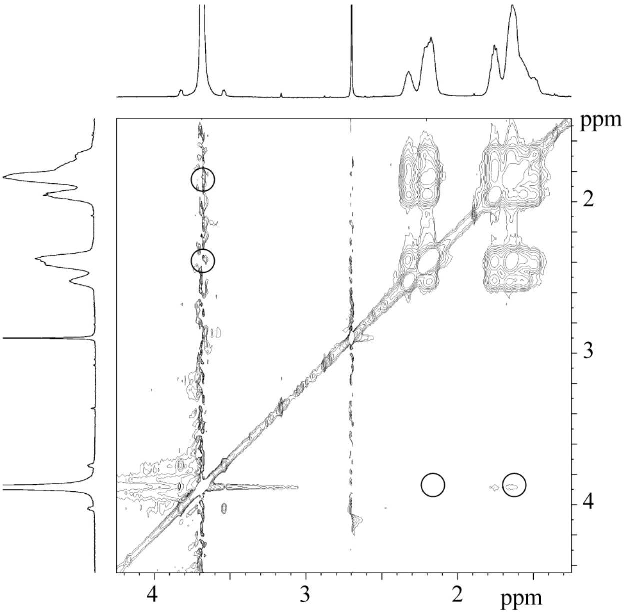

Figure S3. *2D ^1H NMR NOESY contour plot of a 1:1 mixture of PAA_{42}-b-$PAAm_{417}$ and $P2MVP_{42}$-b-PEO_{446} in D_2O at 1mM $NaNO_3$ ($f_+ = 0.50$). Note that the vertical t1 noise line at 3.65 ppm is a result of the relatively large amplitude of the PEO signal compared to that of other protons. Adapted with permission from ref. 19.*

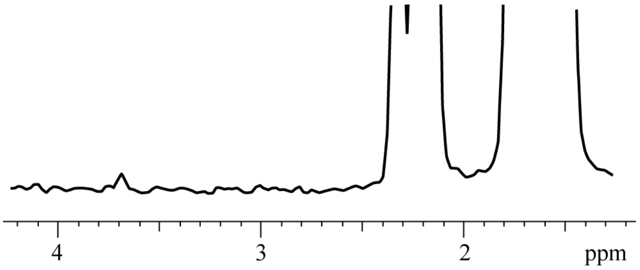

Figure S4. *1.64 ppm line of the 2D ^{1}H NMR NOESY contour plot of a 1:1 mixture of PAA_{42}-b-$PAAm_{417}$ and $P2MVP_{42}$-b-PEO_{446} in D_2O ($f_+ = 0.50$, 1 mM $NaNO_3$).*

2.3 Reversible association and dissociation of Janus Micelles

Table S5 provides the PMC in terms of f_+, as well as the hydrodynamic radius at the PMC, as a function of the p*H* of the polymer stock solutions mixed to form the Janus micelles. The data show that the PMC shifts to higher values with increasing p*H*, as the PAA_{42}-*b*-$PAAm_{417}$ charge density increases.

Table S5. *Hydrodynamic radii, $R_{h,\,90°}$ / nm and preferred micellar composition, PMC, for micelles of PAA_{42}-b-$PAAm_{417}$ and $P2MVP_{42}$-b-PEO_{446} in aqueous solution as a function of pH. pH_+ corresponds to the pH of the $P2MVP_{42}$-b-PEO_{446} stock solution used for C3M preparation; pH_- corresponds to the pH of the PAA_{42}-b-$PAAm_{417}$ stock solution.*

$pH_+ \pm 0.3$	$pH_- \pm 0.3$	PMC	$R_{h,\,90°}$
6.5	6.4	0.39	17.2
7.4	7.5	0.48	17.5
7.7	7.7	0.50	17.6
8.7	8.7	0.52	17.9

We would like to note that upon addition of $NaNO_3$ the hydrodynamic radius of Janus micelles decreases upon increasing ionic strength until a constant value of 7.4 ± 0.5 nm is reached (Figure 7 main text), which is smaller than the hydrodynamic radius observed at 1mM $NaNO_3$ and p*H* < 5.7 in Figure 6 (main text). This can be rationalized as follows: at low p*H* and ionic strength, the soluble complexes (if present) and polymer molecules are highly swollen due to their excess charge, while charge screening and charge neutral conditions lead to less swollen structures at high ionic strength (Figure 7).

2.4 References

* Note that, as observed previously,[16] the resonances corresponding to the P2MVP monomers are broadened beyond the experimental resolution (presumably due to chain rigidity), so that cross peaks between core forming polyelectrolyte segments can not be observed.

1. Voets, I. K.; de Keizer, A.; de Waard, P.; Frederik, P. M.; Bomans, P. H. H.; Schmalz, H.; Walther, A.; King, S. M.; Leermakers, F. A. M.; Cohen Stuart, M. A. *Angewandte Chemie-International Edition* **2006,** 45 (40), 6673-6676.
2. Taton, D.; Wilczewska, A. Z.; Destarac, M. *Macromolecular Rapid Communications* **2001,** 22 (18), 1497-1503.
3. Schmalz, H.; Lanzendorfer, M. G.; Abetz, V.; Müller, A. H. E. *Macromolecular Chemistry and Physics* **2003,** 204 (8), 1056-1071.
4. Salomaa, P.; Schaleger, L. L.; Long, F. A. *Journal of the American Chemical Society* **1964,** 86 (1), 1-7.
5. Voets, I. K.; de Keizer, A.; Cohen Stuart, M. A.; Justynska, J.; Schlaad, H. *Macromolecules* **2007,** 40 (6), 2158-2164.
6. Kline, S. R. *Journal of Applied Crystallography* **2006,** 39 (6), 895-900.
7. Glatter, O. *Journal of Applied Crystallography* **1977,** 10 (5), 415-421.
8. Glatter, O.; Kratky, O., *Small-angle X-ray scattering*. Academic Press: London, 1982.
9. Lindner, P.; Zemb, T., *Neutron, X-rays and Light: Scattering Methods Applied to Soft Condensed Matter* Elsevier: Amsterdam, 2002.
10. Molyneux, P., *Water-soluble synthetic polymers: properties and behavior*. CRC Press: 1982; Vol. 1.
11. Brandrup, J., Immergut, E. H., *Polymer Handbook*. 3 ed.; John Wiley & Sons: 1989.
12. Voets, I. K.; de Keizer, A.; Cohen Stuart, M. A.; de Waard, P. *Macromolecules* **2006,** 39 (17), 5952-5955.
13. Zhang, W. A.; Zhou, X. C.; Li, H.; Fang, Y.; Zhang, G. Z. *Macromolecules* **2005,** 38 (3), 909-914.
14. Burchard, W., Combined static and dynamic light scattering. In *Light Scattering: Principles and Development*, Brown, W., Ed. Clarendon Press: Oxford, 1996.
15. Voets, I. K.; van der Burgh, S.; Farago, B.; Fokkink, R.; Kovacevic, D.; Hellweg, T.; de Keizer, A.; Cohen Stuart, M. A. *Macromolecules* **2007,** 40 (23), 8476-8482.
16. Voets, I. K.; Debuigne, A.; Detrembleur, C.; Jérôme, R.; de Keizer, A.; Cohen Stuart, M. A. **2008,** *submitted.*